

Low-redshift Lyman continuum leaking galaxies with high [O III]/[O II] ratios

Y. I. Izotov^{1,2,3}, G. Worseck⁴, D. Schaerer^{5,6}, N. G. Guseva^{1,2,3}, T. X. Thuan⁷,
K. J. Fricke^{8,3}, A. Verhamme⁵ & I. Orlitová⁹

¹Main Astronomical Observatory, National Academy of Sciences of Ukraine, 27 Zabolotnoho str., Kyiv 03143, Ukraine,
E-mail: izotov@mao.kiev.ua, guseva@mao.kiev.ua

²Bogolyubov Institute for Theoretical Physics, National Academy of Sciences of Ukraine, 14-b Metrolohichna str., Kyiv, 03143, Ukraine

³Max-Planck-Institut für Radioastronomie, Auf dem Hügel 69, D-53121 Bonn, Germany

⁴Institut für Physik und Astronomie, Universität Potsdam, Karl-Liebknecht-Str. 24/25, D-14476 Potsdam, Germany,
E-mail: gworseck@uni-potsdam.de

⁵Observatoire de Genève, Université de Genève, 51 Ch. des Maillettes, 1290, Versoix, Switzerland,
E-mail: daniel.schaerer@unige.ch, anne.verhamme@unige.ch

⁶IRAP/CNRS, 14, Av. E. Belin, 31400 Toulouse, France

⁷Astronomy Department, University of Virginia, P.O. Box 400325, Charlottesville, VA 22904-4325, USA,
E-mail: txt@virginia.edu

⁸Institut für Astrophysik, Göttingen Universität, Friedrich-Hund-Platz 1, D-37077 Göttingen, Germany,
E-mail: kfricke@gwdg.de

⁹Astronomical Institute, Czech Academy of Sciences, Boční II 1401, 141 00, Prague, Czech Republic,
E-mail: orlitova@asu.cas.cz

Accepted XXX. Received YYY; in original form ZZZ

ABSTRACT

We present observations with the Cosmic Origins Spectrograph onboard the *Hubble Space Telescope* of five star-forming galaxies at redshifts z in the range 0.2993 – 0.4317 and with high emission-line flux ratios $O_{32} = [O\ III]\lambda 5007/[O\ II]\lambda 3727 \sim 8 - 27$ aiming to detect the Lyman continuum (LyC) emission. We detect LyC emission in all galaxies with the escape fractions $f_{\text{esc}}(\text{LyC})$ in a range of 2 – 72 per cent. A narrow Ly α emission line with two peaks in four galaxies and with three peaks in one object is seen in medium-resolution COS spectra with a velocity separation between the peaks V_{sep} varying from $\sim 153\text{ km s}^{-1}$ to $\sim 345\text{ km s}^{-1}$. We find a general increase of the LyC escape fraction with increasing O_{32} and decreasing stellar mass M_{\star} , but with a large scatter of $f_{\text{esc}}(\text{LyC})$. A tight anti-correlation is found between $f_{\text{esc}}(\text{LyC})$ and V_{sep} making V_{sep} a good parameter for the indirect determination of the LyC escape fraction. We argue that one possible source driving the escape of ionizing radiation is stellar winds and radiation from hot massive stars.

Key words: (cosmology:) dark ages, reionization, first stars — galaxies: abundances — galaxies: dwarf — galaxies: fundamental parameters — galaxies: ISM — galaxies: starburst

1 INTRODUCTION

Much efforts have been made in recent years to identify the sources of the reionization of the Universe at redshifts $z = 5 - 10$. Two competitive possible sources of ionization, active galactic nuclei (AGN) (Madau & Haardt 2015) and low-mass star-forming galaxies (SFGs) (Ouchi et al. 2009; Wise & Chen 2009; Mitra, Ferrara & Choudhury 2013; Yajima, Choi & Nagamine 2011; Bouwens et al. 2015), were proposed. While there are pro and con arguments on the role of AGN in the reionization of the Universe (e.g. Madau & Haardt 2015;

Hassan et al. 2018; Mitra, Choudhury & Ferrara 2018; Parsa, Dunlop & McLure 2018), their contribution remains uncertain. On the other hand, SFGs can be considered as an important source of ionization only if the escape fraction of their ionizing radiation on average is not less than 10–20 per cent (e.g. Ouchi et al. 2009; Robertson et al. 2013; Dressler et al. 2015; Robertson et al. 2015; Khaire et al. 2016).

Currently, only few reliable Lyman continuum (LyC) leakers with high escape fraction are known at high redshifts, *Ion2* at $z = 3.218$ (Vanzella et al. 2015; de Barros et al. 2016), Q1549-C25 at $z = 3.15$ (Shapley et al. 2016), A2218-

Flanking at $z \approx 2.5$ (Bian et al. 2017), *Ion3* at $z = 3.999$ (Vanzella et al. 2018). The difficulty in the identification of high- z LyC leakers is caused by their faintness, contamination by lower-redshift interlopers and attenuation by partially neutral intergalactic medium (IGM) (e.g., Vanzella et al. 2010, 2012; Inoue et al. 2014; Grazian et al. 2016). To overcome this difficulty it was proposed to study local compact low-mass SFGs as proxies of high- z galaxies (e.g. Izotov et al. 2016a,b). Their stellar masses, metallicities and star-formation rates are similar to those of high- z Lyman-alpha emitting (LAE) galaxies (Izotov et al. 2015, 2016c). A fair fraction of compact SFGs is characterised by high line ratios $O_{32} = [O\ III]\lambda 5007/[O\ II]\lambda 3727 \gtrsim 5$ (Stasińska et al. 2015) indicating that they may contain density-bounded H II regions and be potential LyC leakers as suggested e.g. by Jaskot & Oey (2013) and Nakajima & Ouchi (2014).

Izotov et al. (2016a,b, 2018) selected six compact SFGs at redshifts ~ 0.3 with high $O_{32} \gtrsim 5$ for observations with the *Hubble Space Telescope* (*HST*)/Cosmic Origins Spectrograph (COS). They showed that all six galaxies are LyC leakers with $f_{\text{esc}}(\text{LyC})$ ranging between 6 and 46 per cent. These values are much higher than $f_{\text{esc}}(\text{LyC})$ of $\sim 0 - 4.5$ per cent derived e.g. by Borthakur et al. (2014) and Chisholm et al. (2017) in SFGs with lower O_{32} or with lower equivalent widths of the $H\beta$ emission line (Hernandez et al. 2018).

In this paper we present new *HST*/COS observations of the LyC in 5 compact SFGs with the highest $O_{32} \sim 8 - 27$ ever observed in order to detect ionizing radiation, and examine its behaviour over a wide range of O_{32} . The properties of selected SFGs derived from observations in the optical range are presented in Section 2. The *HST* observations and data reduction are described in Section 3. The surface brightness profiles in the UV range are discussed in Section 4. In Section 5 we compare the *HST*/COS spectra with the extrapolation of the modelled SEDs to the UV range. Ly α emission is considered in Section 6. The escaping Lyman continuum emission is discussed in Section 7 together with the corresponding escape fractions. In Section 8 our results are compared with the LyC escape fractions for other galaxies obtained in some recent studies. We summarize our findings in Section 9.

2 PROPERTIES OF SELECTED GALAXIES DERIVED FROM OBSERVATIONS IN THE OPTICAL RANGE

2.1 Emission-line diagnostic diagrams

Our LyC leaker candidates were selected from the SDSS Data Release 12 (DR12) (Alam et al. 2015) by adopting the selection criteria described in Izotov et al. (2016a,b, 2018). All of them have a compact structure on SDSS images (Fig. 1) and high equivalent widths $EW(H\beta) > 200 \text{ \AA}$ of the $H\beta$ emission line in the SDSS spectra, indicating very recent star formation. These galaxies are located in the upper part of the SFG branch in the Baldwin-Phillips-Terlevich (BPT) diagram (filled stars in Fig. 2a) implying the presence of high-excitation H II regions. Izotov et al. (2016a,b) discussed only galaxies with $O_{32} \sim 5 - 7$. In this paper and in

Izotov et al. (2018) we report observations of galaxies with the considerably larger range of $O_{32} \sim 8 - 27$ (Table 1), aiming to study the applicability of the O_{32} criterion to select galaxies with high escape fractions of ionizing radiation. It is seen in Fig. 2b that the selected galaxies have the highest O_{32} ratios among all local LyC leaking galaxies observed so far.

The SDSS, *GALEX* and *WISE* apparent magnitudes of the selected galaxies are shown in Table 2, indicating that these SFGs are among the faintest low-redshift LyC leakers that have been observed with *HST*.

2.2 Interstellar extinction and element abundances

To derive interstellar extinction and ionized gas metallicity we use the SDSS spectra of the selected galaxies. Our approach is described in detail in Izotov et al. (2016a,b, 2018). In short, we use the prescriptions by Izotov, Thuan & Lipovetsky (1994) to derive galaxy internal interstellar extinction from the observed decrements of hydrogen emission lines. Then the extinction-corrected emission lines are used to derive ionic and total element abundances following the methods described in Izotov et al. (2006) and Guseva et al. (2013).

The emission-line flux densities in the observed SDSS spectra, uncorrected for redshift, were first corrected for the Milky Way extinction with $A(V)_{\text{MW}}$ from the NASA Extragalactic Database (NED)¹, adopting Cardelli, Clayton & Mathis (1989)' reddening law and $R(V)_{\text{MW}} = 3.1$. Then, the flux densities of emission lines at the rest-frame wavelengths were corrected for the internal extinction of galaxies with $R(V)_{\text{int}} = 3.1$ and $A(V)_{\text{int}} = 3.1 \times E(B - V)_{\text{int}}$, where $E(B - V)_{\text{int}} = C(H\beta)_{\text{int}}/1.47$ (Aller 1984).

The emission-line flux densities corrected for both the Milky Way and internal extinction, the rest-frame equivalent widths, the Milky Way $(C(H\beta))_{\text{MW}}$ and internal $(C(H\beta))_{\text{int}}$ extinction coefficients, and extinction-corrected $H\beta$ flux densities are shown in Table 3. The flux densities from Table 3 and the direct T_e method are used to derive physical conditions (the electron temperature and electron number density) and the element abundances in the H II regions. These quantities are shown in Table 4. The oxygen abundances are comparable to those in known low-redshift LyC leakers (Izotov et al. 2016a,b, 2018). The ratios of the neon, magnesium and argon abundances to oxygen abundance are similar to those in dwarf emission-line galaxies (e.g. Izotov et al. 2006; Guseva et al. 2013). On the other hand, the nitrogen-to-oxygen abundance ratios are somewhat elevated, similar to those in other LyC leakers at $z \gtrsim 0.3$.

2.3 Luminosities and stellar masses

The emission-line luminosities and stellar masses of our galaxies were obtained adopting a luminosity distance

¹ NASA/IPAC Extragalactic Database (NED) is operated by the Jet Propulsion Laboratory, California Institute of Technology, under contract with the National Aeronautics and Space Administration.

Table 1. Coordinates, redshifts, distances and O_{32} ratios of selected galaxies

Name	R.A.(2000.0)	Dec.(2000.0)	z	D_L^a	D_A^b	O_{32}
J0901+2119	09:01:45.61	+21:19:27.78	0.2993	1562	925	8.0
J1011+1947	10:11:38.28	+19:47:20.94	0.3322	1763	994	27.1
J1243+4646	12:43:00.63	+46:46:50.40	0.4317	2401	1172	13.5
J1248+4259	12:48:10.48	+42:59:53.60	0.3629	1956	1053	11.8
J1256+4509	12:56:44.15	+45:09:17.01	0.3530	1893	1034	16.3

^aLuminosity distance in Mpc (NED, [Wright 2006](#)).

^bAngular size distance in Mpc (NED, [Wright 2006](#)).

Table 2. Apparent AB magnitudes with errors in parentheses compiled from the SDSS, GALEX and WISE databases

Name	SDSS					GALEX		WISE			
	u (err)	g (err)	r (err)	i (err)	z (err)	FUV (err)	NUV (err)	W1 (err)	W2 (err)	W3 (err)	W4 (err)
J0901+2119	22.01 (0.16)	21.54 (0.05)	20.31 (0.03)	21.94 (0.15)	20.33 (0.12)	22.06 (0.12)	22.17 (0.14)
J1011+1947	21.71 (0.13)	21.26 (0.05)	19.82 (0.02)	21.64 (0.11)	20.52 (0.12)	22.08 (0.50)	21.31 (0.27)
J1243+4646	21.46 (0.11)	21.48 (0.04)	21.63 (0.07)	20.33 (0.03)	21.14 (0.22)	21.31 (0.26)	21.61 (0.24)
J1248+4259	21.55 (0.13)	21.22 (0.05)	20.94 (0.05)	21.23 (0.09)	20.65 (0.20)	21.42 (0.38)	21.16 (0.28)
J1256+4509	22.35 (0.18)	22.01 (0.06)	21.43 (0.05)	22.18 (0.15)	21.51 (0.26)	21.66 (0.30)	21.85 (0.27)	16.29 (0.06)	15.80 (0.11)	12.94 (0.54)	...

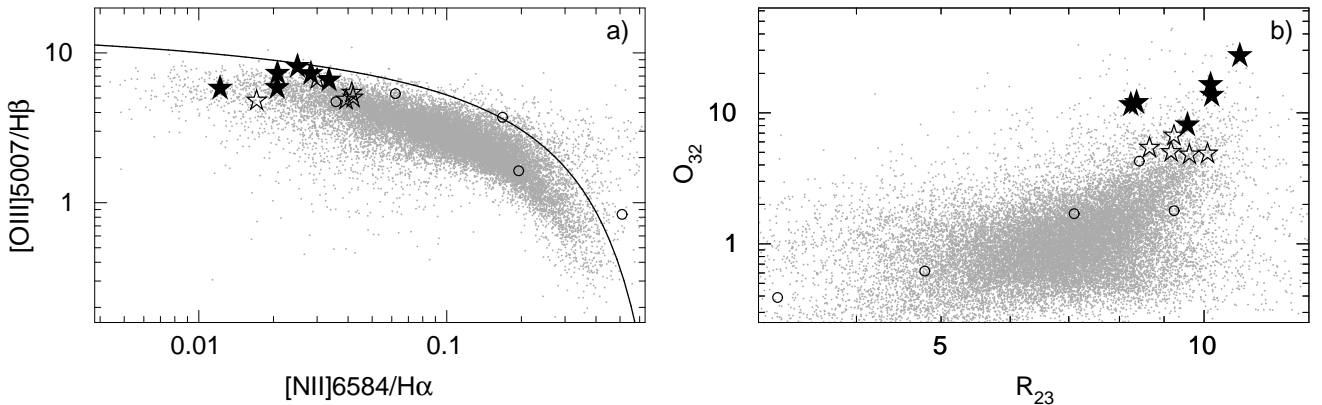

Figure 1. 25 arcsec \times 25 arcsec SDSS composite images of selected galaxies.

Figure 2. a) The Baldwin-Phillips-Terlevich (BPT) diagram ([Baldwin et al. 1981](#)) for SFGs. b) The $O_{32} - R_{23}$ diagram for SFGs where $R_{23} = ([O \text{ II}]3727 + [O \text{ III}]4959 + [O \text{ III}]5007)/H\beta$. The LyC leaking galaxies (this paper) and J1154+2443 ([Izotov et al. 2018](#)) are shown by filled stars in both panels. The location of LyC leaking galaxies by [Borthakur et al. \(2014\)](#); [Chisholm et al. \(2017\)](#) are shown by open circles while LyC leaking galaxies by [Izotov et al. \(2016a,b\)](#) are represented by open stars. The compact SFGs ([Izotov et al. 2016c](#)) are represented by grey dots. The solid line in a) ([Kauffmann et al. 2003](#)) separates SFGs from active galactic nuclei.

Table 3. Extinction-corrected flux densities and rest-frame equivalent widths of the emission lines in SDSS spectra

Line	λ	Galaxy									
		J0901+2119		J1011+1947		J1243+4646		J1248+4259		J1256+4509	
		I^a	EW ^b								
Mg II	2796	10.8±2.4	12	17.2±4.2	8
Mg II	2803	6.5±2.3	7	8.6±3.8	4
[O II]	3727	81.5±4.0	196	29.7±2.3	64	53.7±4.5	81	49.4±3.1	137	44.3±4.4	92
H12	3750	3.3±1.9	9	4.0±2.9	6
H11	3771	5.6±2.8	13	5.1±1.9	13	6.5±2.9	9
H10	3798	7.9±3.3	17	8.0±1.9	21	4.7±2.8	12
H9	3836	6.2±2.9	28	8.9±3.4	19	9.4±1.9	28	7.1±3.3	14
[Ne III]	3869	46.4±2.9	97	49.7±3.0	103	49.1±4.3	98	46.3±2.9	151	55.1±4.7	120
H8+He I	3889	13.5±3.2	33	14.6±2.8	34	20.5±3.8	38	20.4±2.2	87	19.5±3.4	41
H7+[Ne III]	3969	21.6±3.4	52	31.8±2.9	96	39.1±4.1	80	33.9±2.6	124	33.7±4.0	69
H δ	4101	24.2±3.6	56	26.3±3.6	47	26.4±3.4	106	28.1±2.4	112	26.7±3.8	41
H γ	4340	48.0±4.4	97	44.5±3.6	98	47.2±4.2	134	49.6±2.9	228	48.2±4.5	93
[O III]	4363	7.6±1.3	19	14.6±1.7	29	15.5±2.8	45	17.7±1.9	96	16.4±2.9	39
He I	4471	3.9±1.0	14	2.8±0.9	8	3.1±2.1	9	4.2±1.3	18	4.2±2.3	8
H β	4861	100.0±4.9	255	100.0±4.8	237	100.0±5.7	221	100.0±4.0	426	100.0±5.9	253
[O III]	4959	221.2±6.9	741	261.9±7.9	731	240.9±8.9	738	194.0±6.1	851	249.6±9.8	654
[O III]	5007	654.6±26.	1481	807.2±19.	2304	725.9±20.	2057	583.6±14.	2138	723.3±21.	1872
He I	5876	9.6±1.2	35	11.7±1.3	103	10.8±1.3	81	11.4±2.1	52
[O I]	6300	3.2±0.9	10	2.2±0.6	28	2.2±0.7	49
[S III]	6312	4.3±0.8	29
H α	6563	288.8±9.0	831	283.7±8.9	1052	280.9±10.	740	279.8±8.2	2561	280.5±11.	955
[N II]	6583	9.7±1.3	22	7.1±1.1	22	5.8±1.8	10	5.7±0.9	58	7.9±1.2	34
He I	6678	2.6±0.4	30
[S II]	6717	5.5±0.9	57	2.6±0.7	32	3.8±1.3	26
[S II]	6731	5.4±0.9	40	3.1±0.7	40	5.6±1.5	38
He I	7065	5.1±0.8	58
[Ar III]	7136	3.7±0.7	72
$C(H\beta)_{\text{int}}^c$		0.185±0.036		0.135±0.037		0.090±0.044		0.185±0.035		0.095±0.047	
$C(H\beta)_{\text{MW}}^d$		0.038		0.037		0.017		0.032		0.027	
EW(H β) ^b		255±16		237±30		221±10		426±12		253±17	
$I(H\beta)^e$		29.1±1.4		27.0±1.3		14.1±0.8		35.2±1.4		11.4±0.7	

^a $I=100 \times I(\lambda)/I(H\beta)$ where $I(\lambda)$ and $I(H\beta)$ are flux densities of emission lines, corrected for both the Milky Way and internal extinction.

^bRest-frame equivalent width in Å.

^cInternal galaxy extinction coefficient.

^dMilky Way extinction coefficient.

^ein 10^{-16} erg s⁻¹ cm⁻².

(NED, [Wright 2006](#)) with the cosmological parameters $H_0=67.1$ km s⁻¹Mpc⁻¹, $\Omega_\Lambda=0.682$, $\Omega_m=0.318$ ([Ade et al. 2014](#)).

The H β luminosity $L(H\beta)$ and corresponding star-formation rates SFR were obtained from the extinction-corrected H β flux densities using the relation by [Kennicutt \(1998\)](#) for SFR. The star-formation rate should be increased by a factor $1/[1-f_{\text{esc}}(\text{LyC})]$, to take into account the escaping ionizing radiation which is discussed later (see Sect. 7). The SFRs corrected for escaping LyC radiation are shown in Table 5, and they are in the range of values for other LyC leakers. Their specific star formation rates $\text{sSFR} = \text{SFR}/M_\star$ are also similar to sSFRs for other LyC leakers ([Izotov et al. 2016a,b, 2018](#)) and are among the highest known for dwarf SFGs at any redshift ([Izotov et al. 2016c](#)).

We use SDSS spectra of our LyC leakers to fit the spectral energy distribution (SED) and to derive their stellar masses. The fitting method, using a two-component model, is described in [Izotov et al. \(2018\)](#). To take into account the contribution of the young stellar population we adopt a

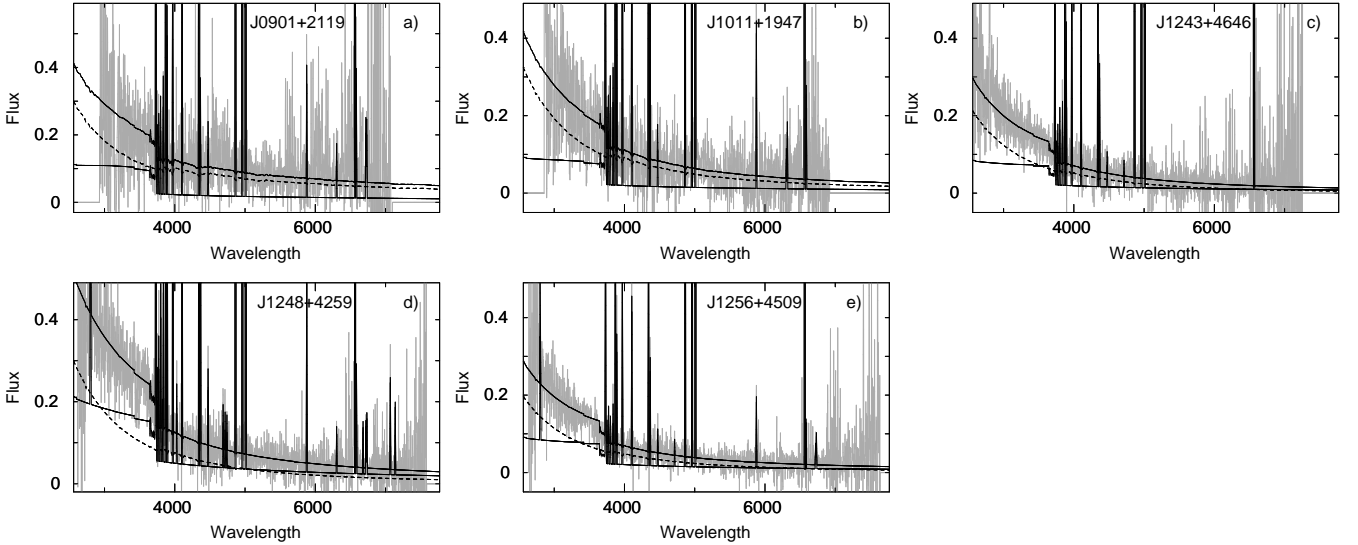
single instantaneous burst. For the older stellar population, we assume that it was formed continuously with a constant SFR. Since the H β equivalent widths of our SFGs are very high, nebular continuum emission must be taken into account; it is determined from the observed H β recombination line flux density and knowing the ISM temperature and density. A χ^2 minimization technique was used to find the best model for the continuum. An additional requirement is that the modelled H β and H α equivalent widths should reproduce the observed values. Several parameters (the starburst age, the age of the older stellar population, the young-to-old stellar population mass ratio) were varied with a Monte-Carlo method to determine the best fit.

To illustrate the quality of our SED fitting we show in Fig. 3 the modelled stellar, nebular and total SEDs superposed to the rest-frame extinction-corrected SDSS spectra. For all galaxies we find very good agreement. We note the considerable contribution ($\sim 20 - 50$ per cent) of nebular emission to the total (stellar+nebular) continuum because of the very high equivalent widths of hydrogen emission lines

Table 4. Electron temperatures, electron number densities and element abundances in H II regions

Galaxy	J0901+2119	J1011+1947	J1243+4646	J1248+4259	J1256+4509
T_e ([O III]), K	12190±780	14610±750	15690±1350	18820±1160	16060±1410
T_e ([O II]), K	12000±720	13770±660	14370±1160	15460±890	14550±1190
T_e ([S III]), K	12170±650	13280±620	14360±1120	17580±970	14720±1170
N_e ([S II]), cm^{-3}	530±600	100 ^a	100 ^a	1180±1180	2690±2690
$O^+/H^+\times 10^5$	1.67±0.18	0.35±0.03	0.56±0.07	0.46±0.03	0.57±0.06
$O^{2+}/H^+\times 10^5$	12.72±0.68	9.42±0.25	7.13±0.21	3.79±0.08	6.78±0.08
$O/H\times 10^5$	14.39±0.70	9.78±0.26	7.68±0.23	4.37±0.11	7.35±0.11
12+log O/H	8.16±0.02	7.99±0.01	7.89±0.01	7.64±0.01	7.87±0.01
$N^+/H^+\times 10^6$	1.15±0.16	0.62±0.10	0.47±0.10	0.40±0.07	0.64±0.15
ICF(N) ^b	7.55	22.48	12.02	8.69	11.25
$N/H\times 10^6$	8.69±1.37	13.95±2.85	5.60±2.06	3.50±0.64	7.16±1.89
log N/O	-1.22±0.07	-0.85±0.09	-1.14±0.16	-1.07±0.12	-1.01±0.12
$Ne^{2+}/H^+\times 10^5$	2.41±0.29	1.44±0.12	1.15±0.13	0.68±0.05	1.21±0.14
ICF(Ne) ^b	1.03	0.97	1.01	1.06	1.01
$Ne/H\times 10^5$	2.47±0.29	1.39±0.11	1.17±0.14	0.71±0.05	1.23±0.14
log Ne/O	-0.75±0.12	-0.85±0.04	-0.82±0.05	-0.79±0.03	-0.78±0.05
$Mg^+/H^+\times 10^6$	0.10±0.02	0.20±0.05
ICF(Mg) ^b	13.73	21.03
$Mg/H\times 10^6$	1.39±0.29	4.17±1.04
log Mg/O	-1.50±0.09	-1.25±0.11
$Ar^{2+}/H^+\times 10^7$	1.17±0.24	...
ICF(Ar) ^b	1.34	...
$Ar/H\times 10^7$	1.58±0.95	...
log Ar/O	-2.44±0.26	...

^aAssumed value.

^bIonization correction factor.

Figure 3. SED fitting of the galaxy SDSS spectra. The rest-frame extinction-corrected spectra are shown by grey lines. The total, nebular and stellar modelled SEDs are shown by thick solid, thin solid and dashed lines, respectively. Flux densities and wavelengths are expressed in 10^{-16} $\text{erg s}^{-1} \text{cm}^{-2} \text{\AA}^{-1}$ and \AA , respectively.

indicating that the emission in the optical range is mostly produced by very young starbursts.

The total stellar masses (young plus old population) and starburst ages (of the young population) of our LyC leakers derived from SED fitting are presented in Table 5. They are similar to those derived for other LyC leakers (Izotov et al. 2016a,b, 2018). The mass of the young stellar population (not shown in Table 5) is typically a small fraction ($\sim 1 - 3$ per cent) of the total stellar mass in all our sources.

3 HST/COS OBSERVATIONS AND DATA REDUCTION

HST/COS spectroscopy of the five LyC leaker candidates was obtained in program GO 14635 (PI: Y. I. Izotov) in December 2017. The program also included J1154+2443, the data of which was already published (Izotov et al. 2018). The observational details are presented in Table 6. As in our previous programs (Izotov et al. 2016a,b), the galaxies were acquired by COS near ultraviolet (NUV) imaging. Since our targets are compact but faint, as based on shallow GALEX imaging, one entire orbit per object was spent for deep NUV imaging and reliable acquisition. The NUV-brightest region of each target was centered in the ~ 2.5 arcsec diameter spectroscopic aperture (Fig. 4). Although the galaxies show some structure with an extended low-surface-brightness (LSB) component and, in the case of J0901+2119, several star-forming knots, their sizes are smaller than the central unvignetted 0.8 arcsec diameter region of the spectroscopic aperture (Fisher et al. 2018). Hence, the galaxy quantities derived from the COS spectra do not require corrections for vignetting.

The spectra were obtained at COS Lifetime Position 4 with the low-resolution grating G140L and medium-resolution grating G160M, applying all four focal-plane offset positions. One orbit of G140L observations of J1011+1947 failed due to a guide star re-acquisition error, shortening the total exposure to 5753 s. However, the shorter exposure was sufficient to achieve our science goals. The 1105 Å setup was used for the G140L grating (COS Lifetime Position 4: wavelength range 1110–2150 Å, resolving power $R \simeq 1400$ at 1150 Å) to include the redshifted LyC emission for all targets. We obtained resolved spectra of the galaxies' Ly α emission lines with the G160M grating ($R \sim 16000$ at 1600 Å), varying the G160M central wavelength with galaxy redshift to cover the emission line and the nearby continuum on one detector segment.

The individual exposures were reduced with the CALCOS pipeline v3.2.1, followed by accurate background subtraction and co-addition with custom software (Worseck et al. 2016). We used the same methods and extraction aperture sizes as in Izotov et al. (2018) to achieve a homogeneous reduction of the galaxy sample observed in our program. We checked the accuracy of our custom correction for scattered light in COS G140L data by comparing the LyC flux densities obtained in the total exposure and in orbital night, respectively (see below). Particularly in the LyC range of the targets the estimated relative background error of 4–10 per cent does not significantly affect our results.

4 SURFACE BRIGHTNESS DISTRIBUTION IN THE NUV RANGE

To determine the surface brightness (SB) profiles of our galaxies we use the COS NUV acquisition images. The method uses the routine *ellipse* in IRAF²/STSDAS³ and is described in detail e.g. in Izotov et al. (2018). The SB profiles (Fig. 5) are common to all LyC leakers studied thus far (this paper, Izotov et al. 2016a,b, 2018) with a sharp increase in the central part because of the presence of the bright star-forming region(s) and a linear decrease (in magnitudes) in the outer part, reminiscent of a disc structure.

The scale lengths α of our galaxies defined in Eq. 1 of Izotov et al. (2016b) are in the range $\sim 1.5 - 1.8$ kpc (Fig. 5), somewhat higher than $\alpha = 0.6 - 1.4$ kpc in other LyC leakers (Izotov et al. 2016a,b, 2018). The corresponding surface densities of star-formation rate in the studied galaxies $\Sigma = \text{SFR}/(\pi\alpha^2)$ are somewhat lower than in other LyC leakers, mainly because of their higher α . Because of the compactness of the bright star-forming region, the half-light radii r_{50} of our galaxies in the NUV are considerably smaller than α (see Table 5). Adopting r_{50} as a measure of the size of these galaxies, the corresponding Σ s are typically two orders of magnitude larger, and comparable to those found for SFGs at high redshifts (Curtis-Lake et al. 2016; Paulino-Afonso et al. 2018; Bouwens et al. 2017). We note for completeness that the star-formation rate surface densities in the LyC leaking galaxy J1154+2443, observed in the course of the same HST GO 14635 program, are $5.1 \text{ M}_{\odot} \text{ yr}^{-1} \text{ kpc}^{-2}$ and $150 \text{ M}_{\odot} \text{ yr}^{-1} \text{ kpc}^{-2}$ for $\alpha = 1.09$ kpc and $r_{50} = 0.2$ kpc, respectively (Izotov et al. 2018), similar to the respective values for the SFGs shown in Table 5.

5 COMPARISON OF THE HST/COS SPECTRA WITH THE MODELLED SEDS IN THE UV RANGE

To derive the fraction of the escaping ionizing radiation, one of the two methods which we use (Izotov et al. 2018) is based on the comparison between the observed flux density in the Lyman continuum range and the intrinsic flux density produced by stellar populations in the galaxy. The latter can be obtained from SED fitting of the SDSS spectra. To verify the quality of our SED fitting, we extrapolate the reddened SEDs to the UV range and compare them with the observed COS spectra in Fig. 6. For comparison, we also show by filled symbols the GALEX FUV and NUV flux densities and the flux densities in the SDSS u, g, r, i, z filters. We find that the spectroscopic and photometric data in the optical range are consistent, indicating that almost all the emission of our galaxies is inside the spectroscopic aperture. Therefore, aperture corrections are not needed. It can be noted that the GALEX FUV photometric flux densities deviate somewhat from the spectroscopic COS flux densities with the two most

² IRAF is distributed by the National Optical Astronomy Observatories, which are operated by the Association of Universities for Research in Astronomy, Inc., under cooperative agreement with the National Science Foundation.

³ STSDAS is a product of the Space Telescope Science Institute, which is operated by AURA for NASA.

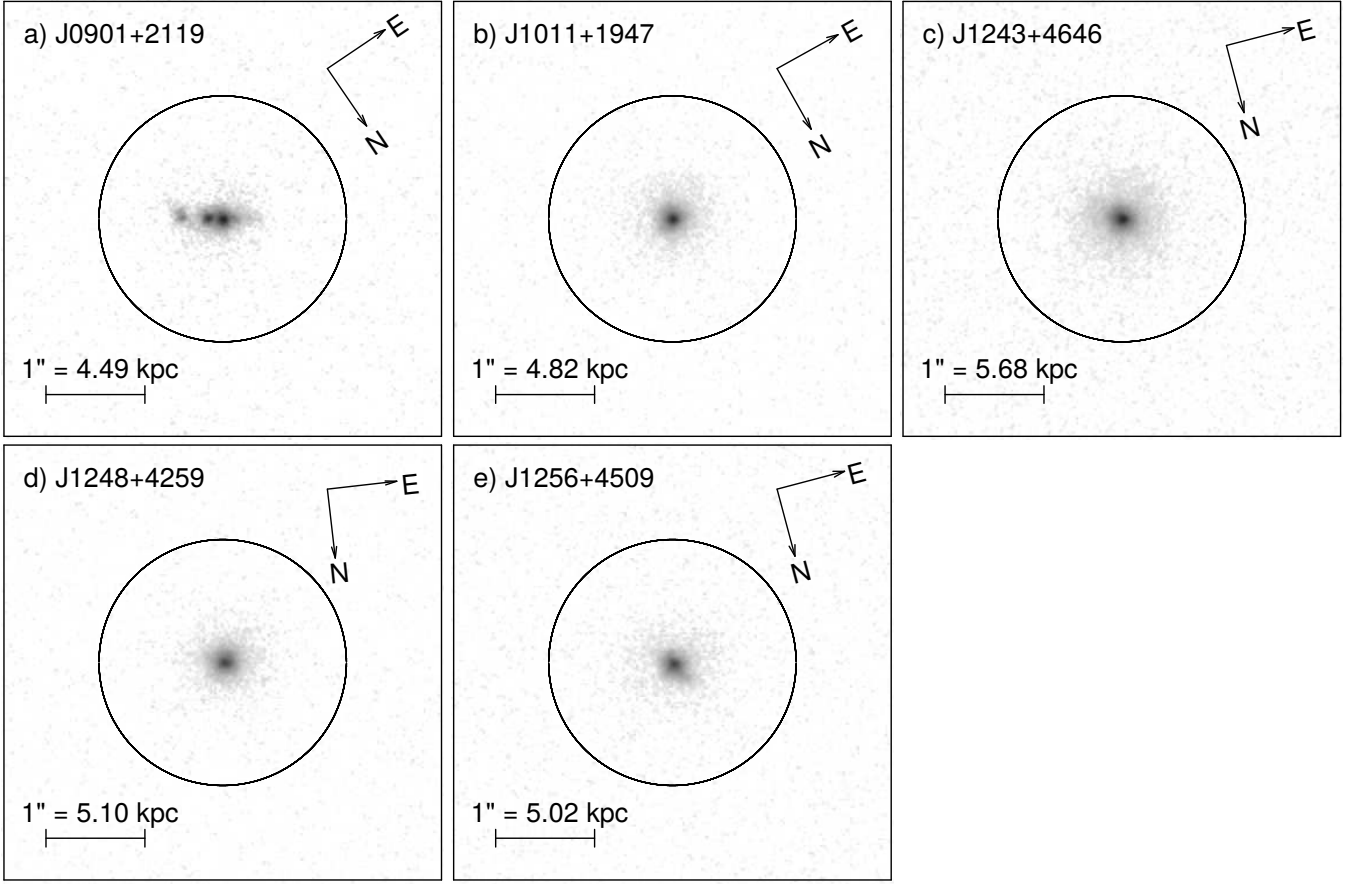


Figure 4. The *HST* NUV acquisition images of the LyC leaking galaxies in log surface brightness scale. The COS spectroscopic aperture with a diameter of 2.5 arcsec is shown in all panels by a circle. The linear scale in each panel is derived adopting an angular size distance.

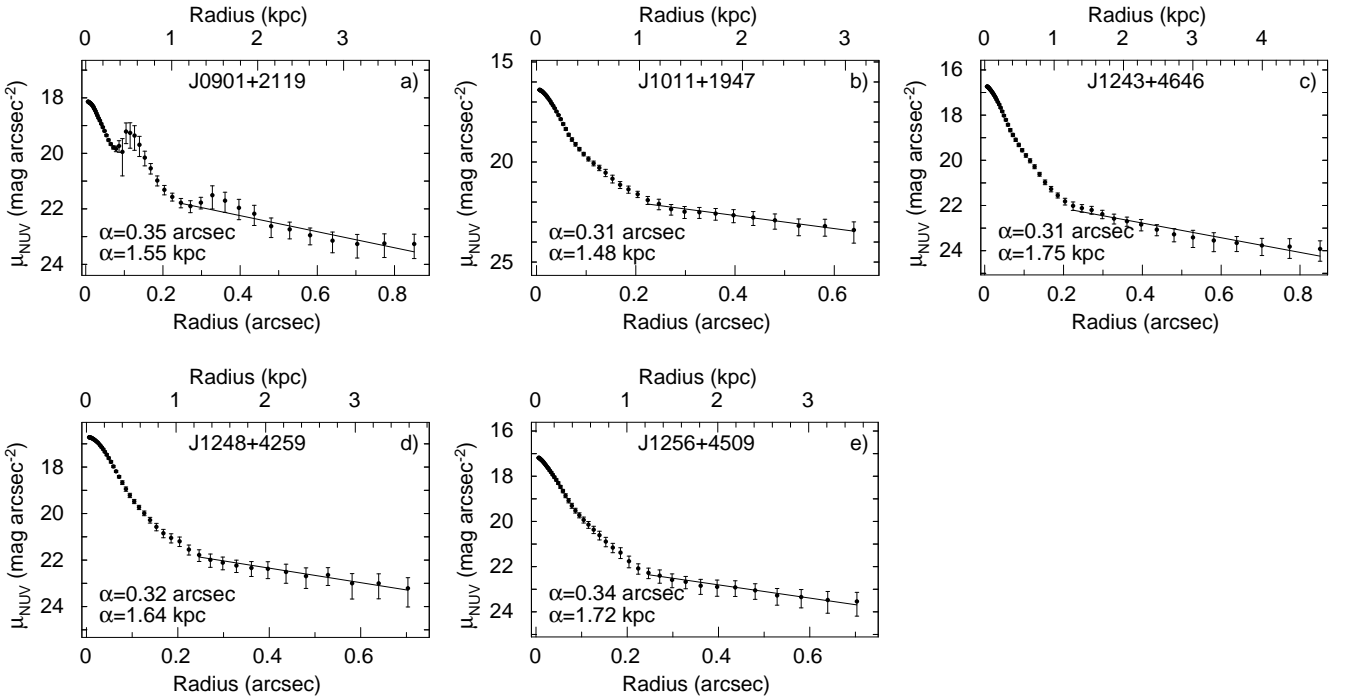


Figure 5. NUV surface brightness profiles of galaxies. The linear fits are shown for the range of radii used for fitting.

Table 5. Integrated characteristics

Name	$M_{\text{FUV}}^{\text{a}}$ (mag)	M_g^{b} (mag)	$\log M_{\star}^{\text{c}}$ ($\log M_{\odot}$)	SB age (Myr)	$\log L(\text{H}\beta)^{\text{d}}$ ($\log \text{erg s}^{-1}$)	SFR $^{\text{e}}$ ($M_{\odot} \text{ yr}^{-1}$)	$\log \text{sSFR}^{\text{e}}$ ($\log \text{yr}^{-1}$)	α^{f} (kpc)	r_{50}^{g} (kpc)	Σ^{h} ($M_{\odot} \text{ yr}^{-1} \text{ kpc}^{-2}$)	Σ^{i}
J0901+2119	-20.02	-19.53	9.8	2.4	41.93	20	-8.5	1.51	0.18	2.7	192
J1011+1947	-20.24	-20.07	9.0	3.4	42.00	25	-7.6	1.48	0.15	4.1	397
J1243+4646	-20.49	-20.46	7.8	2.7	41.99	80	-5.9	1.75	0.19	8.4	719
J1248+4259	-20.60	-20.32	8.2	2.5	42.21	37	-6.6	1.64	0.22	4.3	242
J1256+4509	-19.95	-19.45	8.8	2.4	41.69	18	-7.6	1.72	0.17	2.0	202

^aAbsolute FUV magnitude derived from the intrinsic rest-frame SED.

^bAbsolute SDSS g magnitude corrected for the Milky Way extinction.

^c M_{\star} is the total stellar mass (young + older population).

^d $L(\text{H}\beta)$ is the $\text{H}\beta$ luminosity corrected for the Milky Way and internal extinction.

^eCorrected for the Milky Way and internal extinction, and escaping LyC radiation.

^fExponential disc scale length.

^gGalaxy radius where NUV intensity equal to half of maximal intensity.

^hStar-formation rate surface density assuming galaxy radius equal to α .

ⁱStar-formation rate surface density assuming galaxy radius equal to r_{50} .

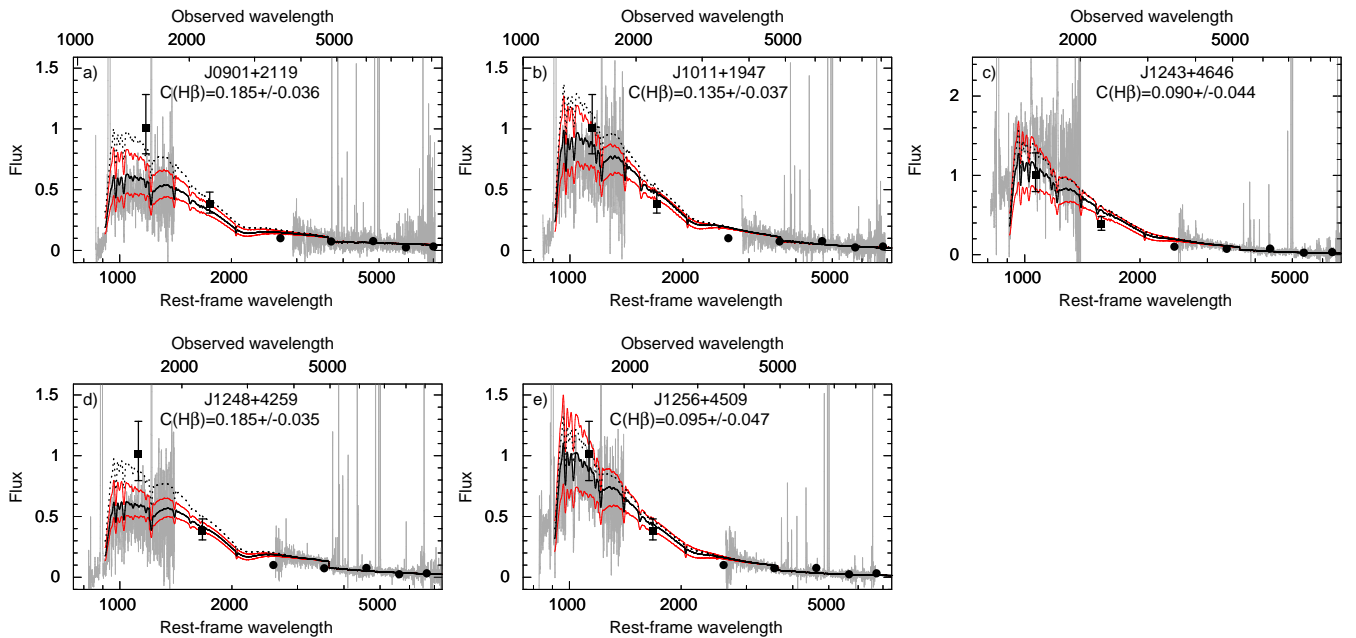


Figure 6. A comparison of the COS G140L and SDSS spectra (grey lines), and photometric data (filled squares and filled circles) with the modelled SEDs. Modelled SEDs reddened by the Milky Way extinction with $R(V)_{\text{MW}} = 3.1$ and internal extinction with $R(V)_{\text{int}} = 3.1$ and 2.4 are shown by thick dotted and solid lines, respectively. The SED variations with the extinction coefficient $C(\text{H}\beta)$ in the 1σ range and $R(V)_{\text{int}} = 2.4$ are shown by red thin lines. Flux densities are in $10^{-16} \text{ erg s}^{-1} \text{ cm}^{-2} \text{ \AA}^{-1}$, wavelengths are in \AA .

deviant cases being J0901+2119 and J1248+4259. The main reason for these deviations is the non-negligible contribution of the redshifted Ly α emission line to the GALEX FUV band. Indeed, a Ly α emission line with an equivalent width in the range $\sim 90 - 250 \text{ \AA}$ (see Table 7) may contribute $\sim 20 - 50$ per cent to the emission in the GALEX FUV band with an effective width of 255 \AA (Rodrigo, Solano & Bayo 2013). However, even for J0901+2119 and J1248+4259 which show the highest Ly α equivalent widths, the FUV photometric and spectroscopic data are consistent within 2σ errors.

We show in Fig. 6 the modelled intrinsic SEDs reddened by adopting the extinction coefficients $C(\text{H}\beta)_{\text{MW}}$ and $C(\text{H}\beta)_{\text{int}}$ (Table 3) and the reddening law by Cardelli et al. (1989) with $R(V)_{\text{MW}} = 3.1$ and $R(V)_{\text{int}} = 2.4$ (thick solid

lines) and 3.1 (dotted lines). For $R(V)_{\text{int}} = 2.4$, we show by red thin solid lines the variations of the reddened SEDs produced by 1σ variations of $C(\text{H}\beta)_{\text{int}}$.

It is seen in Fig. 6 that the models reproduce the SDSS spectra quite well and do not depend on the adopted $R(V)_{\text{int}}$ and variations within 1σ uncertainties of $C(\text{H}\beta)_{\text{int}}$. However, in the UV range there is a stronger dependence of the reddened SEDs on both $R(V)_{\text{int}}$ and $C(\text{H}\beta)_{\text{int}}$ variations. The modelled SEDs reddened with $R(V)_{\text{int}} = 2.4$ reproduce best the COS G140L spectra, in agreement with the conclusions reached by Izotov et al. (2016a,b, 2018) for the other LyC leakers. This implies that the reddening law in the UV range is steeper in our SFGs than in the Milky Way. An exception is J1243+4646, for which the reddening law with $R(V)_{\text{int}} =$

Table 6. *HST*/COS observations

Name	Date	Exposure time (s) (Central wavelength (Å))		
		MIRRORA	G140L	G160M
J0901+2119	2017-12-26	2×1408	5636 (1105)	5636 (1623)
J1011+1947	2017-12-22	2×1408	5753 (1105)	5637 (1577)
J1243+4646	2017-12-19	2×1473	9081 (1105)	5897 (1611)
J1248+4259	2017-12-02	2×1451	5809 (1105)	5809 (1600)
J1256+4509	2017-12-16	2×1473	9082 (1105)	5896 (1600)

3.1 works better, in apparent contradiction with other SFGs. However, an unusual Ly α profile with three peaks (Sect. 6) and a very high $f_{\text{esc}}(\text{LyC})$ (Sect. 7) imply that the interstellar medium in J1243+4646 is clumpy with dust-free holes allowing for some UV continuum radiation to escape through these holes. This could mimick a flatter attenuation law (see eq. 2 in Gazagnes et al. 2018) as compared to that with $R(V)_{\text{int}} = 2.4$.

6 LY α EMISSION

One of the goals of our project is to search empirically for a possible correlation between the amount of escaping LyC radiation and the shape of the Ly α line profile. Verhamme et al. (2017) have proposed that the presence of a double-peaked Ly α profile, with a small peak separation, would be a good indicator of LyC leakage. According to the models of Verhamme et al. (2015), the peak separation decreases with decreasing column density of the neutral gas. This in turn would result in a higher escape fraction of the LyC radiation.

A strong Ly α $\lambda 1216$ Å emission-line is detected in the medium-resolution spectra of all our galaxies (Fig. 7). In general, the profiles show two peaks, labelled by two short vertical lines. This shape is similar to that observed in known LyC leakers (Verhamme et al. 2017) and in some other galaxies (Jaskot & Oey 2014; Henry et al. 2015; Yang et al. 2017). The Ly α profile of J1243+4646 is more complex and consists of three peaks. Interestingly, it is quite similar to that of the $z = 3.999$ LyC leaker *Ion3* recently discovered by Vanzella et al. (2018) and of the lensed galaxy Sunburst Arc at $z = 2.4$ (Rivera-Thorsen et al. 2017). Some parameters of Ly α emission are presented in Table 7. For J1243+4646, two separations are given. It is seen that the separation between peaks varies in a range between ~ 150 km s $^{-1}$ and ~ 350 km s $^{-1}$ with the lowest values for J1243+4646 and J1256+4509. These are also among the lowest values found for low-redshift LyC leakers. The Ly α profiles of these two galaxies indicate that they are efficient LyC leakers, similar to the galaxy J1154+2443 (Izotov et al. 2018). This is examined quantitatively in Sect. 7.3.

7 ESCAPING LYMAN CONTINUUM RADIATION

7.1 Observed and intrinsic Lyman continuum flux densities

Blow-ups of the LyC spectral region are illustrated in Fig. 8 showing clearly that Lyman continuum emission is significantly detected in the spectra of all galaxies. The average flux densities are shown by filled circles with 3σ statistical error bars. The short thick solid lines indicate wavelength ranges used for averaging. The observed LyC emission flux densities $I_{\text{obs}}(\text{total})$ should be corrected for the Milky Way extinction to derive the escaping flux densities $I_{\text{esc}}(\text{total})$. The extinction-corrected average LyC flux densities $I_{\text{esc}}(\text{total})$ are shown by the dotted horizontal lines in Fig. 8. The corresponding measurements are summarized in Table 8.

We also show in Table 8 the observed LyC flux densities $I_{\text{obs}}(\text{shadow})$ derived from the exposures during periods with considerably lower night sky emission. In general, $I_{\text{obs}}(\text{shadow})$ is somewhat lower than $I_{\text{obs}}(\text{total})$, implying some contribution of the geocoronal scattered light to the flux densities in observations with the total exposures. In any case both measurements are consistent within the 2σ errors for all galaxies.

To derive the escape fraction of ionizing radiation in our sources we use two methods to determine the intrinsic emission in the Lyman continuum, following Izotov et al. (2016a,b, 2018). We here briefly illustrate the steps of the first method, which uses the SED fits combining the SDSS optical spectra and the COS UV spectra described above to predict the LyC radiation.

The observed G140L total-exposure spectra (grey lines) and predicted intrinsic SEDs (thick dash-dotted lines) are shown in Fig. 9, together with the reddened intrinsic SEDs (thick solid lines). The predicted SEDs are obtained from fitting optical SDSS spectra which are corrected for the Milky Way extinction at observed wavelengths, adopting $A(V)(\text{MW})$ from the NED and for the internal extinction at rest-frame wavelengths, the preferred UV attenuation law (i.e. R_V discussed above), and the extinction coefficients $C(\text{H}\beta)_{\text{int}}$ derived from the hydrogen Balmer decrement.

The thin dash-dotted lines show the intrinsic SEDs derived by adopting extinction coefficients $C(\text{H}\beta)_{\text{int}} \pm \sigma[C(\text{H}\beta)_{\text{int}}]$ where $\sigma[C(\text{H}\beta)_{\text{int}}]$ are 1σ errors of $C(\text{H}\beta)_{\text{int}}$. It is seen that the intrinsic LyC flux density depends on the adopted extinction coefficient, being higher for higher $C(\text{H}\beta)_{\text{int}}$. This is due to the fact that a higher extinction-corrected H β flux density corresponds to a higher number of ionizing photons.

7.2 LyC escape fraction

To derive $f_{\text{esc}}(\text{LyC})$ Izotov et al. (2016a,b) and Izotov et al. (2018) used the ratio of the escaping flux densities I_{esc} to the intrinsic flux densities I_{mod} of the Lyman continuum:

$$f_{\text{esc}}(\text{LyC}) = \frac{I_{\text{esc}}(\lambda)}{I_{\text{mod}}(\lambda)}, \quad (1)$$

where λ is the mean wavelength of the range used for averaging of the LyC flux density (see Table 8). They proposed two methods to derive the intrinsic flux densities I_{mod} . The

Table 7. Parameters for the Ly α emission line

Name	$A(\text{Ly}\alpha)_{\text{MW}}^{\text{a}}$	I^{b}	$\log L^{\text{c}}$	EW^{d}	$V_{\text{sep}}^{\text{e}}$
J0901+2119	0.210	106.2 \pm 2.3	42.49	179 \pm 3.9	345.0 \pm 12.5
J1011+1947	0.202	123.4 \pm 2.6	42.66	121 \pm 3.1	276.4 \pm 5.4
J1243+4646	0.092	180.3 \pm 2.8	43.09	98 \pm 1.9	143.4 \pm 4.0
J1248+4259	0.174	150.0 \pm 2.7	42.83	256 \pm 5.2	163.8 \pm 5.7
J1256+4509	0.147	88.4 \pm 2.1	42.58	86 \pm 3.2	283.8 \pm 15.9

^aMilky Way extinction at the observed wavelength of the Ly α emission line in mags

adopting [Cardelli et al. \(1989\)](#) reddening law with $R(V)=3.1$.

^bFlux density in 10^{-16} erg s $^{-1}$ cm $^{-2}$ measured in the COS spectrum and corrected for the Milky Way extinction.

^c L is Ly α luminosity in erg s $^{-1}$ corrected for the Milky Way extinction.

^dRest-frame equivalent width in \AA .

^eLy α peak separation in km s $^{-1}$.

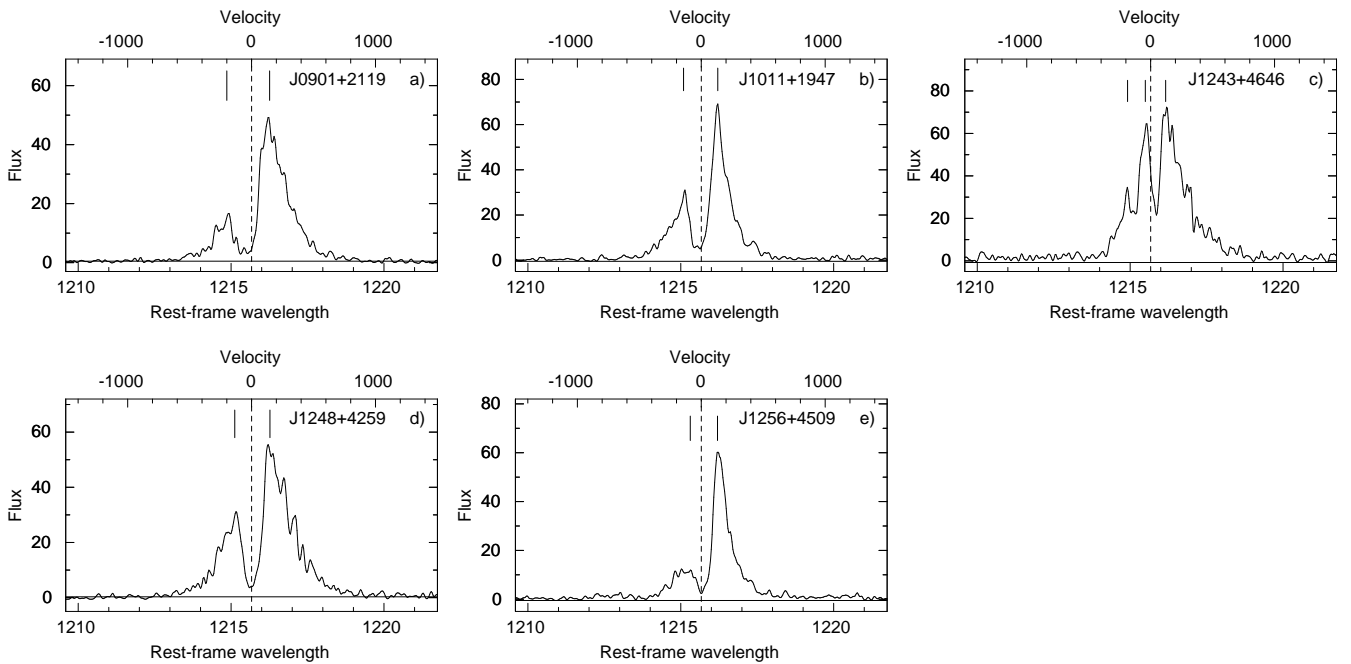


Figure 7. Ly α profiles. Vertical dashed lines and short vertical solid lines indicate the centres of profiles and profile peaks, respectively. Flux densities are in 10^{-16} erg s $^{-1}$ cm $^{-2}$ \AA^{-1} , wavelengths are in \AA and velocities are in km s $^{-1}$.

first method is based on the SED fitting as described above. The relation between the luminosities of hydrogen recombination lines and the number of ionizing photons emitted per unit time, $N(\text{LyC})$, is used in the second method. The details of both methods are described by [Izotov et al. \(2018\)](#).

Using Eq. 1, we derive the escape fractions $f_{\text{esc}}(\text{LyC})$ by both methods accounting for the uncertainties of the observed monochromatic LyC flux densities and those of the extinction coefficients $C(\text{H}\beta)_{\text{int}}$. For most of our sources the two methods give escape fractions which agree within the uncertainties. The derived $f_{\text{esc}}(\text{LyC})$ (Table 8) vary over a wide range and are very high for J1243+4646 and J1256+4509 with escape fractions of ~ 72 per cent and 38 per cent, respectively. These values, together with $f_{\text{esc}}(\text{LyC}) = 46$ per cent for J1154+2443 ([Izotov et al. 2018](#)), are among the highest known for low- and high-redshift galaxies. They are far above the average LyC escape fractions for SFGs of \sim

10 – 20 per cent needed to fully reionize the Universe at redshifts $z > 5$.

7.3 Indicators of high $f_{\text{esc}}(\text{LyC})$

The direct detection of LyC emission in low-redshift star-forming galaxies is a difficult task. At the moment, only *HST* can be used for that purpose. Although our targets are relatively bright in the UV (M_{UV} close to M_{UV}^* of the high- z luminosity function) and the COS G140L observations are fairly short (1 – 2 orbits), relatively few galaxies at $z \gtrsim 0.3$ can be observed directly in the LyC in this manner. Therefore, reasonable indirect indicators of LyC leakage are needed to build a larger sample for statistical studies. We consider below some possible indicators.

[Guseva et al. \(2004\)](#), [Jaskot & Oey \(2013\)](#) and [Nakajima & Ouchi \(2014\)](#) proposed that a high O_{32} ratio can be an indication of density-bounded H II regions and

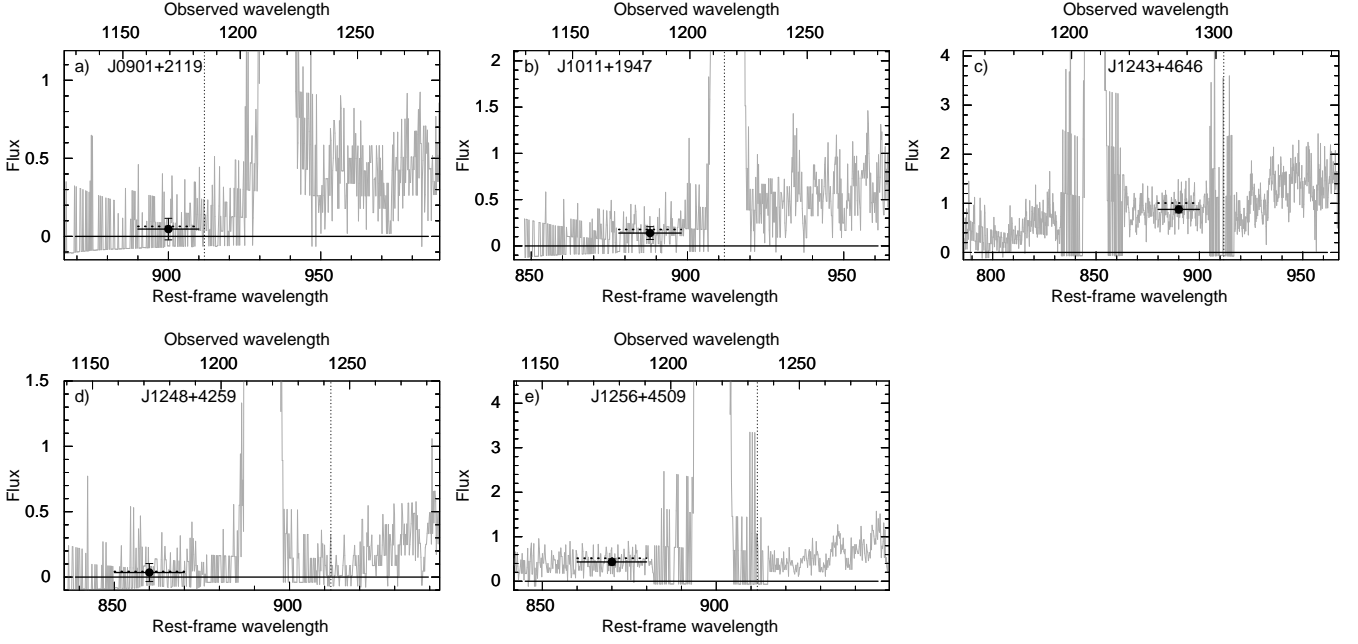


Figure 8. Segments of COS G140L spectra with the Lyman continuum. Filled circles show the average observed values with the 3σ error bars. The observed mean LyC flux densities and flux densities after correction for the Milky Way extinction are indicated by short solid horizontal lines and short dotted horizontal lines, respectively. The Lyman limit at 912\AA rest-frame wavelength is indicated by dotted vertical lines. Zero flux densities are shown by horizontal lines. Flux densities are in $10^{-16} \text{ erg s}^{-1} \text{ cm}^{-2} \text{\AA}^{-1}$, wavelengths are in \AA .

Table 8. LyC escape fraction

Name	λ_0^a (\AA)	$A(\text{LyC})_{\text{MW}}^b$ (mag)	$I_{\text{mod}}^{c,d}$	$I_{\text{obs}}(\text{total})^{c,e}$	$I_{\text{obs}}(\text{shadow})^{c,f}$	$I_{\text{esc}}(\text{total})^{c,g}$	f_{esc}^h (per cent)	f_{esc}^i (per cent)
J0901+2119	890-910	0.280	2.47 ± 0.22	0.055 ± 0.013	0.039 ± 0.018	0.067 ± 0.016	2.7 ± 0.7	2.1 ± 0.3
J1011+1947	878-898	0.268	1.65 ± 0.20	0.146 ± 0.015	0.113 ± 0.023	0.187 ± 0.019	11.4 ± 1.8	6.2 ± 0.7
J1243+4646	880-900	0.118	1.29 ± 0.17	0.874 ± 0.020	0.914 ± 0.096	0.936 ± 0.021	72.6 ± 9.7	72.3 ± 7.2
J1248+4259	850-870	0.235	2.30 ± 0.15	0.040 ± 0.012	0.033 ± 0.015	0.050 ± 0.015	2.2 ± 0.7	1.4 ± 0.4
J1256+4509	860-880	0.197	1.38 ± 0.20	0.438 ± 0.019	0.326 ± 0.068	0.525 ± 0.022	38.0 ± 5.7	46.0 ± 5.6

^aRest-frame wavelength range in \AA used for the determination of the LyC flux density.

^bMilky Way extinction at the mean observed wavelengths of the range used for the determination of the LyC flux density.

The Cardelli et al. (1989) reddening law with $R(V) = 3.1$ is adopted.

^cin $10^{-16} \text{ erg s}^{-1} \text{ cm}^{-2} \text{\AA}^{-1}$.

^dLyC flux density derived from the modelled SED.

^eObserved LyC flux density derived from the spectrum with total exposure.

^fObserved LyC flux density derived from the spectrum with shadow exposure.

^gObserved LyC flux density in the spectrum with total exposure which is corrected for the Milky Way extinction.

^h $I_{\text{esc}}(\text{total})/I_{\text{mod}}$, where I_{mod} is derived from SED (first method).

ⁱ $I_{\text{esc}}(\text{total})/I_{\text{mod}}$, where I_{mod} is derived from $H\beta$ flux density (second method).

thus of high $f_{\text{esc}}(\text{LyC})$. At low redshifts the $[\text{O II}]\lambda 3727$ and $[\text{O III}]\lambda 5007$ emission lines are seen in the optical range. Their flux densities are available for large samples of SFGs. Now with our new LyC leakers we have in hand a sample of sixteen galaxies with a wide range of $O_{32} \sim 0.5 - 27$ (Leitert et al. 2013; Borthakur et al. 2014; Leitherer et al. 2016; Izotov et al. 2016a,b, 2018, this paper). The relation between $f_{\text{esc}}(\text{LyC})$ and O_{32} is presented in Fig. 10a. Although there is a trend of increasing $f_{\text{esc}}(\text{LyC})$ with increasing of O_{32} , the spread of $f_{\text{esc}}(\text{LyC})$ at high O_{32} is large. Furthermore, the LyC escape fraction in the galaxy J1011+1947 with the highest O_{32} is relatively low. This is in line with the conclusions of Izotov et al. (2017) that

a high O_{32} is a necessary but not sufficient condition for escaping ionizing radiation. The O_{32} ratio also depends on other parameters, such as ionization parameter, hardness of ionizing radiation and metallicity of the H II region. The spread of galaxies in the $f_{\text{esc}}(\text{LyC}) - O_{32}$ diagram can also be caused by their different orientations relative to the observer and by inhomogeneous LyC leakage. For example, it was demonstrated by Thuan & Izotov (1997) that the low-metallicity galaxy SBS 0335-052E with a high $O_{32} \sim 15$ shows very strong Ly α absorption in its UV spectrum, indicating an extremely high neutral hydrogen column density $N(\text{H I}) \sim 7 \times 10^{21} \text{ cm}^{-2}$ along the line of sight, preventing leakage of LyC radiation. However, recently

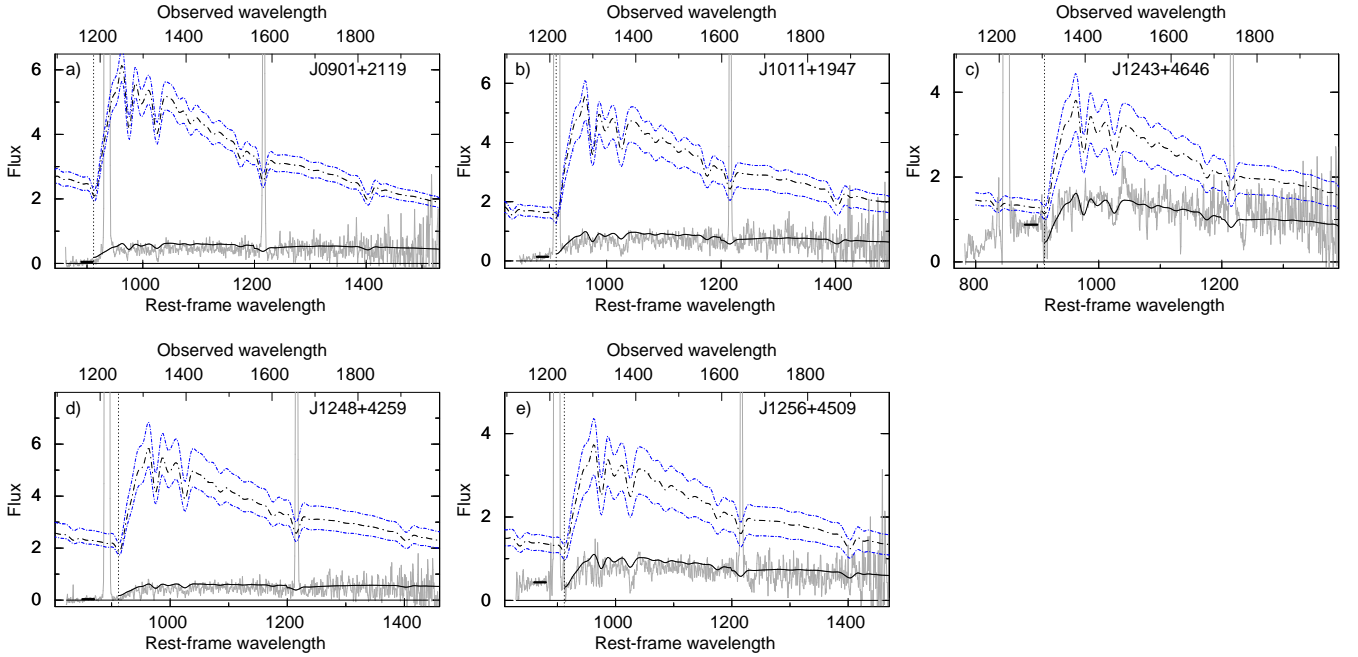


Figure 9. COS G140L spectra of our sources (grey lines) superposed by the modelled SEDs (thick solid lines), reddened by both the internal and Milky Way extinctions. The unreddened (intrinsic) SEDs are shown by the thick dash-dotted lines. The variations of intrinsic SEDs are shown by thin dash-dotted lines for 1σ uncertainties of $C(H\beta)_{\text{int}}$ (see Table 3). $R(V)_{\text{int}} = 2.4$ and $R(V)_{\text{MW}} = 3.1$ are adopted in all panels except for the galaxy J1243+4646 for which $R(V)_{\text{int}} = 3.1$ is adopted. Lyman limit at the rest-frame wavelength 912\AA is indicated by dotted vertical lines. Zero flux densities are represented by solid horizontal lines. Flux densities are in $10^{-16} \text{ erg s}^{-1} \text{ cm}^{-2} \text{\AA}^{-1}$, wavelengths are in \AA .

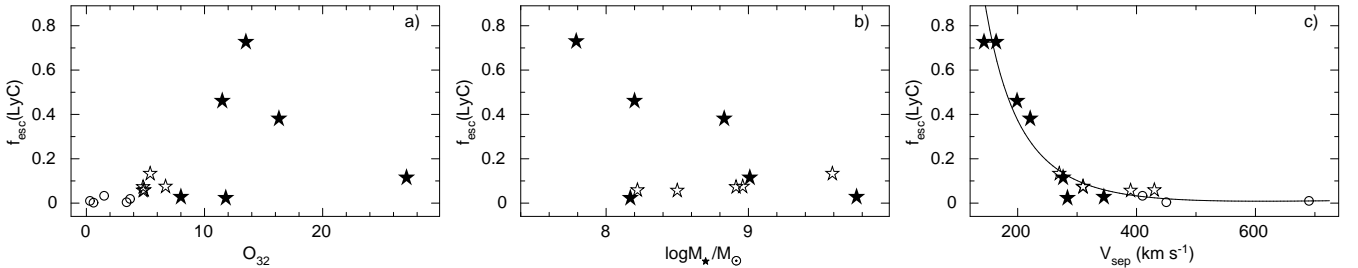


Figure 10. Relations between the Lyman continuum escape fraction $f_{\text{esc}}(\text{LyC})$ in low-redshift LyC leaking galaxies and **a)** the $[\text{O III}]\lambda 5007/[\text{O II}]\lambda 3727$ emission-line ratio, **b)** the stellar mass M_{\star} , and **c)** the separation V_{sep} between the $\text{Ly}\alpha$ profile peaks. LyC leakers from Izotov et al. (2018) and this paper are shown by filled stars, the LyC leakers from Izotov et al. (2016a,b) are represented by open stars and other LyC leaking galaxies from Leitert et al. (2013), Borthakur et al. (2014) and Leitherer et al. (2016) with $f_{\text{esc}}(\text{LyC})$ derived by Chisholm et al. (2017) are shown by open circles. The two separations in the galaxy J1243+4646 with the highest $f_{\text{esc}}(\text{LyC})$ are shown (see Fig. 7c and Table 7).

Herenz et al. (2017) discovered holes in the H I envelope of this galaxy probably oriented nearly perpendicularly to the line of sight, which could allow for LyC leakage in some directions.

It has also been suggested that $f_{\text{esc}}(\text{LyC})$ tends to be higher in low-mass galaxies (Wise et al. 2014; Trebitsch et al. 2017). Stellar masses M_{\star} are available for a large number of star-forming galaxies because observations with ground-based telescopes are sufficient for their determination. In particular, SDSS spectra can be used for that. We show in Fig. 10b the relation between $f_{\text{esc}}(\text{LyC})$ and stellar mass M_{\star} . It is seen that there is a tendency of increasing $f_{\text{esc}}(\text{LyC})$ with decreasing M_{\star} , although a large scatter is present. New observations of LyC leakers with lower log

$M_{\star}/M_{\odot} < 8.0$ are needed to verify the suggested increase of $f_{\text{esc}}(\text{LyC})$ with decreasing M_{\star} .

The profile of the $\text{Ly}\alpha$ emission line can also be used as an indirect indicator of the LyC leakage. This indicator is most useful because it can be applied to nearby low-mass galaxies for which direct observations of the LyC are not possible because of their low redshift. Verhamme et al. (2017) and Izotov et al. (2018) found a tight dependence of $f_{\text{esc}}(\text{LyC})$ on the separation V_{sep} between the peaks of the $\text{Ly}\alpha$ emission line in LyC leakers. Adding the new LyC leakers discussed in this paper extends the relation to higher $f_{\text{esc}}(\text{LyC})$ and lower V_{sep} and strengthens it considerably (Fig. 10c). The regression line (solid line) to this relation

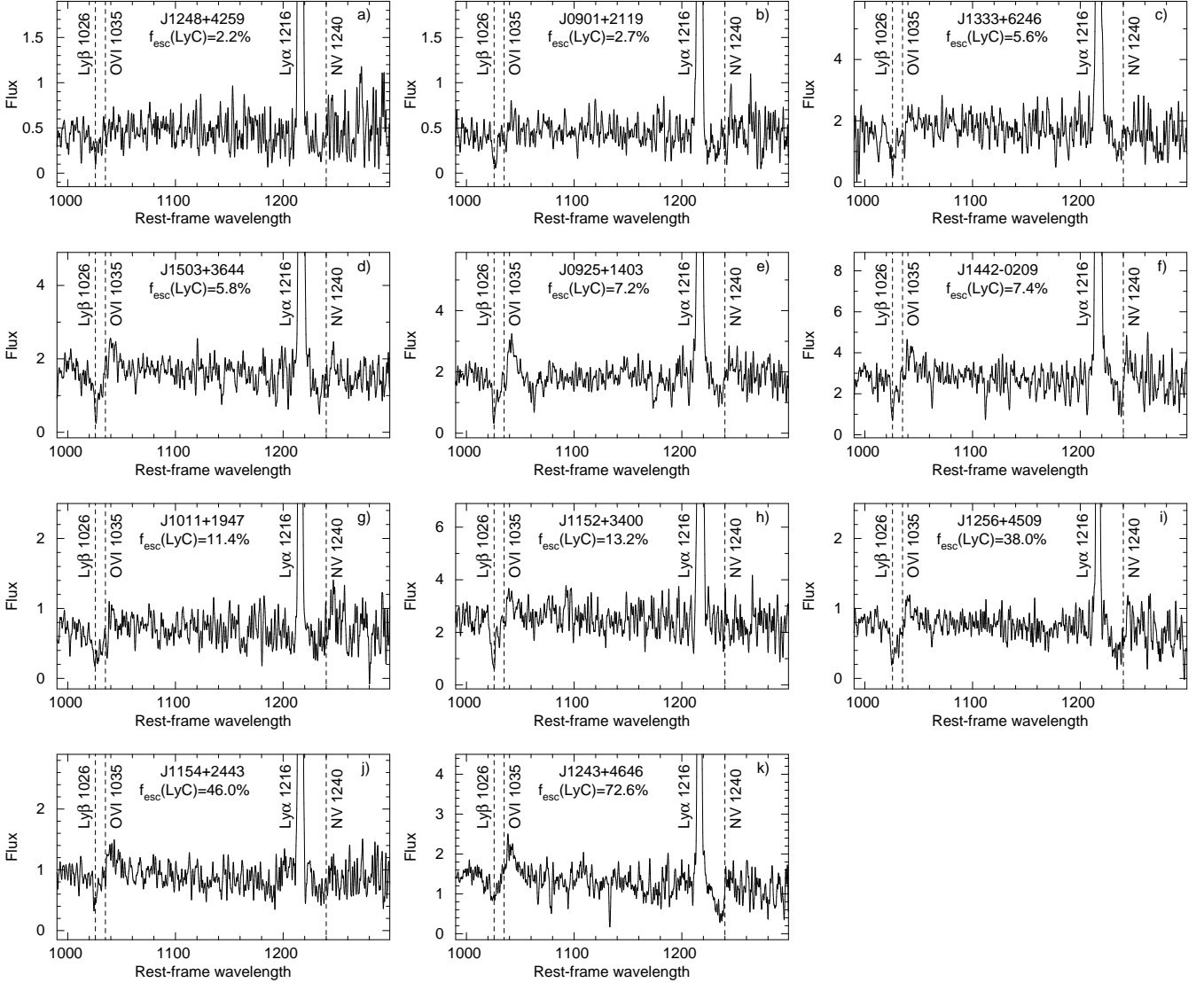


Figure 11. Segments of COS G140L spectra with broad stellar lines O VI $\lambda 1035\text{\AA}$ and N V $\lambda 1240\text{\AA}$ for all LyC leakers studied by Izotov et al. (2016a,b, 2018) and in this paper. The centres of these lines and of the Ly β line are indicated by vertical dashed lines. The spectra are ordered according to the $f_{\text{esc}}(\text{LyC})$ values from lowest (top) to highest (bottom). Flux densities are in 10^{-16} erg s^{-1} $\text{cm}^{-2}\text{\AA}^{-1}$, wavelengths are in \AA .

is

$$f_{\text{esc}}(\text{LyC}) = \frac{3.23 \times 10^4}{V_{\text{sep}}^2} - \frac{1.05 \times 10^2}{V_{\text{sep}}} + 0.095, \quad (2)$$

where V_{sep} is in km s^{-1} . We note that the relation Eq. 2 is empirical and is incorrect at very small Ly α peak separations resulting in $f_{\text{esc}}(\text{LyC}) > 1$ at $V_{\text{sep}} \lesssim 140$ km s^{-1} .

Both the LyC and Ly α escaping radiation are determined by the column density of the neutral gas in LyC leaking galaxies (e.g. Verhamme et al. 2015, 2017) implying a tight relation between V_{sep} and $f_{\text{esc}}(\text{LyC})$, as it is in Fig. 10c. This relation described by Eq. 2 should constitute a strong constraint for constructing radiative transfer and kinematical models which simultaneously reproduce $f_{\text{esc}}(\text{LyC})$ and the Ly α profile.

Another potential indicator is shown in Fig. 11, where we present segments of COS G140L spectra of the LyC leak-

ers we have studied previously and in this paper, in the wavelength range $\sim 1000 - 1300\text{\AA}$ which includes the stellar lines O VI $\lambda 1035$ and N V $\lambda 1240$ with P-Cygni profiles, indicative of stellar winds from hot massive stars (this paper, Izotov et al. 2016a,b, 2018). The spectra are shown in order of increasing $f_{\text{esc}}(\text{LyC})$. The stellar lines are very weak in spectra of galaxies with lowest $f_{\text{esc}}(\text{LyC}) \lesssim 5$ per cent (Figs. 11a-c). In spectra of all other LyC leakers with higher $f_{\text{esc}}(\text{LyC})$ these lines are clearly seen, implying that, in principle, stellar lines with P-Cygni profiles from hot massive stars could also be considered as indicators of LyC leakage.

Finally, a coherent analysis of UV absorption lines (including H lines of the Lyman series and metallic lines such as Si II $\lambda 1260$) and the UV attenuation also provide a consistent and accurate measure of the Lyman continuum escape fraction, as shown in detail by Gazagnes et al. (2018) and Chisholm et al. (2018).

Overall we conclude that the most reliable and simple empirical indicator of LyC leakage is the separation between the peaks of the Ly α profile. There are, however, several problems with the use of this indicator. First, the Ly α line must be resolved for the study of its profile. Additionally, for low-redshift galaxies, UV observations are needed. Finally, at redshifts corresponding to the epoch of recombination, Ly α is effectively absorbed by the intergalactic neutral medium.

8 DISCUSSION

We now briefly compare our sources with those studied in other recent papers. [Hernandez et al. \(2018\)](#) have observed seven $z \sim 0.3$ star-forming galaxies with the COS spectrograph targeting also the Lyman continuum. No LyC emission is detected, translating to an absolute LyC escape fraction of $f_{\text{esc}}(\text{LyC}) = 0.4^{+10}_{-0.4}$ per cent from the stacked (combined) spectrum, excluding thus strong LyC leakage. The galaxies were selected from the COSMOS survey as star-forming galaxies, applying a few additional selection criteria. Both the rest-frame UV (Ly α) and optical emission lines of their sources are relatively weak compared to our galaxies, as measured by their equivalent widths which are quite low, $\text{EW}(\text{H}\beta) \sim 7 - 77 \text{ \AA}$, compared to our median value of $\sim 220 \text{ \AA}$. Correspondingly, the specific star formation rate sSFR of these galaxies is fairly modest (sSFR $\sim 10^{-9.7}$ to $10^{-8.1} \text{ yr}^{-1}$). Comparing these properties with those of our sources, the LyC non-detection in the galaxies of [Hernandez et al. \(2018\)](#) may not be surprising. Indeed, the strong LyC leakers detected so far are all characterized by their compactness, very strong emission lines and very high sSFR. These properties are also typical of those of normal $z > 6$ star-forming galaxies, making our compact leakers good analogs of the sources of cosmic reionization, as shown by [Schaerer et al. \(cf. 2016\)](#), whereas the galaxies observed by [Hernandez et al. \(2018\)](#) are more typical of low- z non-compact star-forming galaxies.

A recent study by [Naidu et al. \(2018\)](#) has examined Lyman continuum escape in $z \sim 3.5$ galaxies with strong [O III] emission lines, finding a low escape fraction of < 10 per cent and questioning the usefulness of high O₃₂ ratios for finding strong LyC emitters. Using an overdensity at $z = 3.42 - 3.58$, these authors have selected 73 star-forming galaxies to search for LyC emission probed by a deep VIMOS U -band image. Again, the LyC remains undetected both for the individual sources and in stacks, from which they derive a 1σ upper limit of $f_{\text{esc}}(\text{LyC}) < 6.3 \pm 0.7$ per cent on the relative LyC escape fraction of the total sample. They also examine “strong [O III]” emitters, finding $f_{\text{esc}}(\text{LyC}) < 8.2 \pm 0.8$ per cent for this subsample of 54 sources with rest-frame $\text{EW}([\text{O III}]\lambda 5007) \sim 400 \text{ \AA}$ and an estimated O₃₂ ~ 4.3 . From this, [Naidu et al. \(2018\)](#) conclude that their result raises questions about the reliability of extreme $\text{EW}([\text{O III}]\lambda 5007)$ and O₃₂ as effective tracers of LyC escape.

A quick comparison with the properties of the $z \sim 0.3$ galaxies studied in our work ([Izotov et al. 2016a, 2018](#), and the present work) shows that our sources have significantly stronger emission lines ($\text{EW}([\text{O III}]\lambda 5007) \sim 1400 - 2100 \text{ \AA}$ compared to $\sim 400 \text{ \AA}$ rest-frame) and higher O₃₂ line ratios (extinction-corrected O₃₂ $\gtrsim 5$ compared to ~ 4 before extinction correction). At O₃₂ < 4 we do not find any source with

absolute LyC escape fractions above ~ 2 per cent, which is compatible with their non-detections. In short, the result of [Naidu et al. \(2018\)](#) does not contradict our findings and hence does not exclude that galaxies with very strong emission lines and a high ratio O₃₂ are Lyman continuum emitters, as we found at $z \sim 0.3$, although there is no tight correlation between O₃₂ and LyC escape in our sample.

Another recent study examined the LyC escape fraction of emission line-selected $z \sim 2.5$ galaxies, finding 1σ upper limits on the absolute escape fraction of $f_{\text{esc}} < 6 - 14$ per cent ([Rutkowski et al. 2017](#)), where the latter value is applicable to a subsample of 13 sources with O₃₂ > 5 . As mentioned by these authors, their observations are not deep enough to detect escape fractions of $\sim 2 - 15$ per cent as measured for the majority of our sources (8 out of 11). On the other hand, the three galaxies with the highest LyC escape fractions in our sample have all fairly low stellar masses $M_{\star} \lesssim 10^9 M_{\odot}$, clearly outside the mass range of the galaxies observed by [Rutkowski et al. \(2017\)](#), which have masses $M_{\star} \sim 10^9 - 10^{10.5} M_{\odot}$, with a median mass of $M_{\star} \sim 10^{9.7} M_{\odot}$. Hence their results are also compatible with our findings. For comparison, the stellar masses of the low- z galaxies observed by [Hernandez et al. \(2018\)](#) span a fairly large range with the bulk of the sources between $M_{\star} \sim 10^{9.5} - 10^{10} M_{\odot}$, as found from the catalog of [Laigle et al. \(2016\)](#). These results combined with our findings indicate that Lyman continuum leakage is probably more common and higher in galaxies of low mass.

From the available observations, we conclude that compact and intensely star-forming galaxies with sufficiently strong optical emission lines and a high O₃₂ line ratio are excellent Lyman continuum leaker candidates. Furthermore, the $z \sim 0.3$ galaxies we have studied are outliers of the galaxy population at low redshift, but their properties are fairly typical of galaxies in the early Universe (cf. [Schaerer et al. 2016](#)). It is therefore straightforward to suggest that the average Lyman continuum escape fraction of a galaxy at a given stellar mass should increase with increasing redshift, as ultimately needed to explain cosmic reionization. In addition, LyC escape could also be more frequent and/or the average escape fraction higher in low mass galaxies ($10^7 < M_{\star} < 10^9 M_{\odot}$), as suggested by numerical simulations (e.g. [Wise et al. 2014; Trebitsch et al. 2017](#)).

9 CONCLUSIONS

We present new *Hubble Space Telescope (HST)* Cosmic Origins Spectrograph (COS) observations of five compact star-forming galaxies (SFG) with high O₃₂ = [O III] $\lambda 5007$ /[O II] $\lambda 3727$ flux density ratios in the range $\sim 8 - 27$, and in the redshift range $z = 0.2993 - 0.4317$. We use these data to study the Ly α emission and the escaping Lyman continuum (LyC) radiation of these SFGs. This study is an extension of the work reported earlier in [Izotov et al. \(2016a,b, 2018\)](#). Our main results are summarized as follows:

1. LyC leakage, i.e. emission of Lyman continuum radiation, is detected in all five galaxies. The highest escape fractions, $f_{\text{esc}}(\text{LyC}) = 72 \pm 10$ per cent and 38 ± 6 per cent, are found in J1243+4646 and J1256+4509, respectively. These values are among the highest known for LyC leakers at any redshift.

2. A Ly α emission line with two peaks is observed in the spectra of four galaxies, and a Ly α emission line with three peaks is detected in the spectrum of J1243+4646, the object with the highest $f_{\text{esc}}(\text{LyC})$. A strong anti-correlation between $f_{\text{esc}}(\text{LyC})$ and the peak velocity separation of the Ly α profile is found, as suggested earlier by Izotov et al. (2018).

3. We find that a high O₃₂ ratio is a necessary but not sufficient condition for a large amount of Lyman continuum radiation escaping from SFGs. Instead, the most reliable selection criterion for LyC leakers is the peak separation of the Ly α profile V_{sep} which is strongly anti-correlated to the LyC escape fraction $f_{\text{esc}}(\text{LyC})$, as qualitatively predicted by the radiation transfer simulations of Verhamme et al. (2015).

4. A bright compact star-forming region (with the exception of J0901+2119 which shows 2 fainter knots of star formation in addition to the main star-forming region) is seen in the COS near ultraviolet (NUV) acquisition images. The surface brightness at the outskirts can be approximated by an exponential disc, with a scale length of $\sim 1.48 - 1.75$ kpc, indicating that all our LyC leakers may be dwarf disc systems.

5. Our galaxies are characterized by stellar masses $M_{\star} \sim 10^{7.8} - 10^{9.8} M_{\odot}$ and high star-formation rates in the range $\text{SFR} \sim 18 - 80 M_{\odot} \text{ yr}^{-1}$. Their specific star formation rates are among the highest found in low-redshift LyC leakers. The metallicities of our galaxies are low, ranging from $12 + \log \text{O}/\text{H} = 7.64$ to 8.16.

We have discovered a class of galaxies in the local Universe which are leaking ionizing radiation, some with very high escape fractions ($\gtrsim 40$ per cent). They share many properties of high-redshift galaxies, indicating that stars in high-redshift galaxies may have reionized the Universe. The dominance of very young ($\lesssim 3$ Myr) stars in their intense star-forming events suggests that stellar winds and radiation from massive stars may be an important source driving the escape of ionizing radiation. These local galaxies are ideal laboratories for pursuing the investigation of the mechanisms responsible for the escape of ionizing radiation from galaxies.

ACKNOWLEDGEMENTS

Based on observations made with the NASA/ESA *Hubble Space Telescope*, obtained from the data archive at the Space Telescope Science Institute. STScI is operated by the Association of Universities for Research in Astronomy, Inc. under NASA contract NAS 5-26555. Support for this work was provided by NASA through grant number HST-GO-14635.002-A from the Space Telescope Science Institute, which is operated by AURA, Inc., under NASA contract NAS 5-26555. G.W. has been supported by the Deutsches Zentrum für Luft- und Raumfahrt (DLR) through grant number 50OR1720. I.O. acknowledges grants GACR 14-20666P and 17-06217Y of the Czech National Foundation. Funding for SDSS-III has been provided by the Alfred P. Sloan Foundation, the Participating Institutions, the National Science Foundation, and the U.S. Department of Energy Office of Science. The SDSS-III web site is <http://www.sdss3.org/>. SDSS-III is managed by the Astrophysical Research Consortium for the Participating Institutions of the SDSS-III

Collaboration. GALEX is a NASA mission managed by the Jet Propulsion Laboratory. This research has made use of the NASA/IPAC Extragalactic Database (NED) which is operated by the Jet Propulsion Laboratory, California Institute of Technology, under contract with the National Aeronautics and Space Administration.

REFERENCES

- Ade P. A. R. et al., 2014, *A&A*, 571, A16
 Alam S. et al., 2015, *ApJS*, 219, 12
 Aller L. H., 1984, *Physics of Thermal Gaseous Nebulae*. Dordrecht: Reidel
 Baldwin J. A., Phillips M. M., Terlevich R., 1981, *PASP*, 93, 5
 Bian F., Fan X., McGreer I., Cai Z., Jiang L., 2017, *ApJ*, 837, 12
 Borthakur S., Heckman T. M., Leitherer C., Overzier R. A., 2014, *Science*, 346, 216
 Bouwens R. J., Illingworth G. D., Oesch P. A., Caruana J., Holwerda B., Smit R., Wilkins S., 2015, *ApJ*, 811, 140
 Bouwens R. J., Illingworth G. D., Oesch P. A., Atek H., Lam D., Stefanon M., 2017, *ApJ*, 843, 41
 Cardelli J. A., Clayton G. C., Mathis J. S., 1989, *ApJ*, 345, 245
 Chisholm J., Orlitová I., Schaerer D., Verhamme A., Worseck G., Izotov Y. I., Thuan T. X., Guseva N. G., 2017, *A&A*, 605, A67
 Chisholm J. et al., 2018, *A&A*, in press; preprint arXiv:1803.03655
 Curtis-Lake E. et al., 2016, *MNRAS*, 457, 440
 de Barros S. et al., 2016, *A&A*, 585, A51
 Dressler A., Henry A., Martin C. L., Sawicki M., McCarthy P., Villaneuva E., 2015, *ApJ*, 806, 19
 Fischer W. J. et al., 2018, *Cosmic Origins Spectrograph Instrument Handbook*, Version 10.0. Baltimore: STScI
 Gazagnes S., Chisholm J., Schaerer D., Verhamme A., Rigby J. R., Bayliss M., 2018, *A&A*, in press; preprint arXiv:1802.06378
 Grazian A. et al., 2016, *A&A*, 585, A48
 Green J. C. et al., 2012, *ApJ*, 744, 60
 Grimes J. P. et al., 2009, *ApJ*, 181, 272
 Guseva N. G., Papaderos P., Izotov Y. I., Noeske K. G., Fricke K. J., 2004, *A&A*, 421, 519
 Guseva N. G., Izotov Y. I., Fricke K. J., Henkel C., 2013, *A&A*, 555, A90
 Hassan S., Davé R., Mitra S., Finlator K., Ciardi B., Santos M. G., 2018, *MNRAS*, 473, 227
 Henry A., Scarlata C., Martin C. S., Erb D., 2015, *ApJ*, 809, 19
 Herenz E. C., Hayes M., Papaderos P., Cannon J. M., Bik A., Melinder J., Östlin G., 2017, *A&A*, 604, 99
 Hernandez S., Leitherer C., Boquien M., Buat V., Burgarella D., Calzetti D., Noll S., 2018, *MNRAS*, in press; preprint arXiv:1804.09721
 Inoue A. K., Shimizu I., Iwata I., Tanaka M., 2014, *MNRAS*, 442, 1805
 Izotov Y. I., Thuan T. X., Lipovetsky V. A., 1994, *ApJ*, 435, 647
 Izotov Y. I., Stasińska G., Meynet G., Guseva N. G., Thuan T. X., 2006, *A&A*, 448, 955
 Izotov Y. I., Guseva N. G., Fricke K. J., Henkel C., 2015, *MNRAS*, 451, 2251
 Izotov Y. I., Orlitová I., Schaerer D., Thuan T. X., Verhamme A., Guseva N. G., Worseck G., 2016a, *Nature*, 529, 178
 Izotov Y. I., Schaerer D., Thuan T. X., Worseck G., Guseva N. G., Orlitová I., Verhamme A., 2016b, *MNRAS*, 461, 3683
 Izotov Y. I., Guseva N. G., Fricke K. J., Henkel C., 2016c, *MNRAS*, 462, 4427
 Izotov Y. I., Thuan T. X., Guseva N. G., 2017, *MNRAS*, 471, 548
 Izotov Y. I., Schaerer D., Worseck G., Guseva N. G., Thuan T.

- X., Verhamme A., Orlitová I., Fricke K. J., 2018, MNRAS, 474, 4514
- Jaskot A. E., Oey M. S., 2013, ApJ, 766, 91
- Jaskot A. E., Oey M. S., 2014, ApJ, 791, L19
- Kauffmann G. et al., 2003, MNRAS, 341, 33
- Kennicutt R. C., Jr., 1998, ARA&A, 36, 189
- Khairé V., Srianand R., Choudhury T. R., Gaikwad P., 2016, MNRAS, 457, 4051
- Laigle C. et al., 2016, ApJS, 224, 24
- Leitet E., Bergvall N., Hayes M., Linné S., Zackrisson E., 2013, A&A, 553, A106
- Leitherer C., Hernandez S., Lee J. C., Oey M. S., 2016, ApJ, 823, L64
- Madau P., Haardt F., 2015, ApJ, 813, L8
- Mitra S., Ferrara A., Choudhury T. R., 2013, MNRAS, 428, L1
- Mitra S., Choudhury T. R., Ferrara A., 2018, MNRAS, 473, 1416
- Naidu R. P., Forrest B., Oesch P. A., Tran K.-V. H., Holden B. P., 2018, MNRAS, in press; preprint arXiv:1804.06845
- Nakajima K., Ouchi M., 2014, MNRAS, 442, 900
- Ouchi M. et al., 2009, ApJ, 706, 1136
- Parsa S., Dunlop J.S., McLure R. J., 2018, MNRAS, 474, 2904
- Paulino-Afonso A. et al., 2018, MNRAS, 476, 5479
- Rivera-Thorsen T. E. et al., 2017, A&A, 608, L4
- Robertson B. E. et al., 2013, ApJ, 768, 71
- Robertson B. E., Ellis R. S., Furlanetto S. R., Dunlop J. S., 2015, ApJ, 802, L19
- Rodrigo C., Solano E., Bayo A., 2013, The SVO Filter Profile Service, <http://ivoa.net/documents/Notes/SVOFPS/index.html>
- Rutkowski M. G. et al., 2017, ApJ, 841, L27
- Schaerer D., Izotov Y. I., Verhamme A., Orlitová I., Thuan T. X., Worseck G., Guseva, N. G., 2016, A&A, 591, L8
- Shapley A. E., Steidel C. C., Strom A. L., Bogosavljević M., Reddy N. A., Siana B. Mostardi R. E., Rudie G. C., 2016, ApJ, 826, L24
- Stasińska G., Izotov Y., Morisset C., Guseva N., 2015, A&A, 576, A83
- Thuan T. X., Izotov Y. I., 1997, ApJ, 477, 661
- Trebitsch M., Blaizot J., Rosdahl J., Devriendt J., Slyz A., 2017, MNRAS, 470, 224
- Vanzella E. et al., 2010, ApJ, 725, 1011
- Vanzella E. et al., 2012, ApJ, 751, 70
- Vanzella E. et al., 2015, A&A, 576, A116
- Vanzella E. et al., 2018, MNRAS, 476, L15
- Verhamme A., Orlitová I., Schaerer D., Hayes M., 2015, A&A, 578, A7
- Verhamme A., Orlitová I., Schaerer D., Izotov Y., Worseck G., Thuan T. X., Guseva N., 2017, A&A, 597, A13
- Wise J. H., Cen R., 2009, ApJ, 693, 984
- Wise J. H., Demchenko V. G., Halicek M. T., Norman M. L., Turk M. J., Abel T., Smith B. D., 2014, MNRAS, 442, 2560
- Worseck G., Prochaska J. X., Hennawi J. F., McQuinn M., 2016, ApJ, 825, 144
- Wright E. L., 2006, PASP, 118, 1711
- Yajima H., Choi J.-H., Nagamine K., 2011, MNRAS, 412, 411
- Yang H. et al., 2017, ApJ, 844, 171

This paper has been typeset from a $\text{\TeX}/\text{\LaTeX}$ file prepared by the author.